Two-Element Uplink Array Loss Statistics Derived from Site Test Interferometer Phase Data for the Goldstone Climate: Initial Study Results

David D. Morabito* and Larry D'Addario†

ABSTRACT. — Site test interferometers (STIs) have been deployed at the Venus and Apollo antenna sites in Goldstone, California, to assess the suitability of Goldstone as an uplink array site, and to statistically characterize atmospheric-induced phase fluctuations for application to Goldstone array link scenarios. The phase decorrelation data extracted from the STIs are filtered to remove long-period trends due to satellite motion and instrumental drift. The remaining fluctuation energy is dominated by the troposphere over timescales ranging from ~ second to several hundred seconds. The fluctuation in phase delay (or pathlength difference) statistics derived from these data can be used to infer power loss for particular array configurations after appropriate scaling to elevation angle, frequency, and array element spacing. The phase decorrelation data from both Goldstone STIs have been mapped into two-element phasing loss (amplitude fades) referenced at a frequency of 7.15 GHz and at an elevation angle of 20 deg to assess statistical behavior. This article thus predicts phasing loss statistics that would be measured by a two-element array at Goldstone.

I. Introduction

In order to address the problem of replacing the aging monolithic 70-m-diameter antennas of the Deep Space Network (DSN) for future deep-space missions, NASA is exploring the use of arraying smaller-diameter antennas in order to achieve comparable or better sensitivity for downlink and effective power for uplink. These antennas would need to be separated by up to hundreds of meters and would then be susceptible to unequal pathlength variations induced by atmospheric turbulence. Such fluctuations can reduce the coherence of a set of antennas being used as a phased array. These variations can be measured in real time for a downlink array where a sufficiently strong reference signal is available, and thus atmospheric fluctuations could be corrected for in the processing along with other time-varying

* Communications Architectures and Research Section.

† Tracking Systems and Applications Section.

The research described in this publication was carried out by the Jet Propulsion Laboratory, California Institute of Technology, under a contract with the National Aeronautics and Space Administration.

contributions such as changing geometry. However, in the case of uplink, such reference signals are not always available, and thus the loss induced by such effects will need to be characterized. Early demonstration work where the Apollo 34-m subnet was configured to perform uplink arraying at X-band[1] with a spacecraft suggests that tropospheric contributions to amplitude loss are very small, much less than a dB [1].

There is an effort underway to build, test, and deploy site test interferometers (STIs) at each of the three DSN complexes to statistically characterize such atmospheric decorrelation effects over typical array element separations. These instruments consist of two small-diameter antennas and associated electronics separated by ~200 m with optical fiber connections carrying local oscillator (LO) and intermediate frequency (IF) signals between each element and a central electronics equipment rack. The STI antennas continuously observe signals emitted by a geostationary satellite and produce data that contain information on the phase differences of the signals received by both antennas. An STI thus monitors the difference in pathlength between a distant source and two points on Earth, thereby providing a way of measuring atmospheric phase fluctuations over spatial distances that are comparable to element separations of possible microwave phased array configurations. The effect of these fluctuations on the operation of an array varies between sites due to climate and altitude, and at any one site diurnally, seasonally, and with passage of weather systems. It is desired to operate an STI for several years in order to establish a sufficient database for a reliable statistical characterization of these effects at a given site. These data can thus be used to characterize the suitability of sites for deploying an uplink array, or their statistics can be used in link characterizations for current or proposed future missions using a given array site. The statistics can be used to estimate phasing loss for a given array configuration by appropriate scaling of the STI elevation angle, frequency, and element spacing to those of the array [2–4]. The STI data can also be used to provide real-time information when deployed next to an array being used for uplink when a downlink signal reference is not available.

II. Instrumentation Description

The first STI at Goldstone, California, was deployed at the Venus (DSS-13) antenna site (latitude of 35.07 deg N and longitude of 243.206 deg E) in May 2007 [2–8]. The Venus STI is composed of two 1.2-m-diameter antennas (and associated equipment) separated by ~256 m in an east–west configuration. These antennas are continuously pointed at ANIK F2 (orbital longitude of 111.1 deg W), a Canadian broadcast satellite in geostationary orbit, at an elevation angle of 48.5 deg. The 20.2-GHz beacon tone emitted by ANIK F2 is used as the signal source for this STI. A stable oscillator signal is distributed to the two antennas, and the phases of the received tones relative to the oscillator are separately and simultaneously measured over each 1-s interval. The difference of these measurements is the raw observable of the instrument that is recorded in the output file for each 1-day period. The phase differencing of signals between elements and subsequent corrections occur during post-processing after the files have been downloaded, thus effectively producing "interferometric" phase in non–real time.

[1] In this article, "X-band" refers to the 7.145- to 7.235-GHz band that is allocated to Earth-to-space transmissions in the Space Research Service by the International Telecommunications Union.

The first year of Venus STI statistics was acquired from May 2007 to April 2008. The second year of data acquisition spanned from August 2008 to July 2009, and the third year spanned from August 2009 to July 2010. A fourth year of data acquisition started in August 2010. The initial results are documented in a series of papers [5–8]. Figure 1 displays the locations of the STI antenna elements at the Venus complex at Goldstone. One element is located next to the 34-m diameter R&D BWG antenna and the other element is located next to the Venus operations control building. The deployment logistics and ongoing data analysis for the Venus STI were collaborative efforts between propagation experimenters at NASA Glenn Research Center (GRC) and the Jet Propulsion Laboratory (JPL).

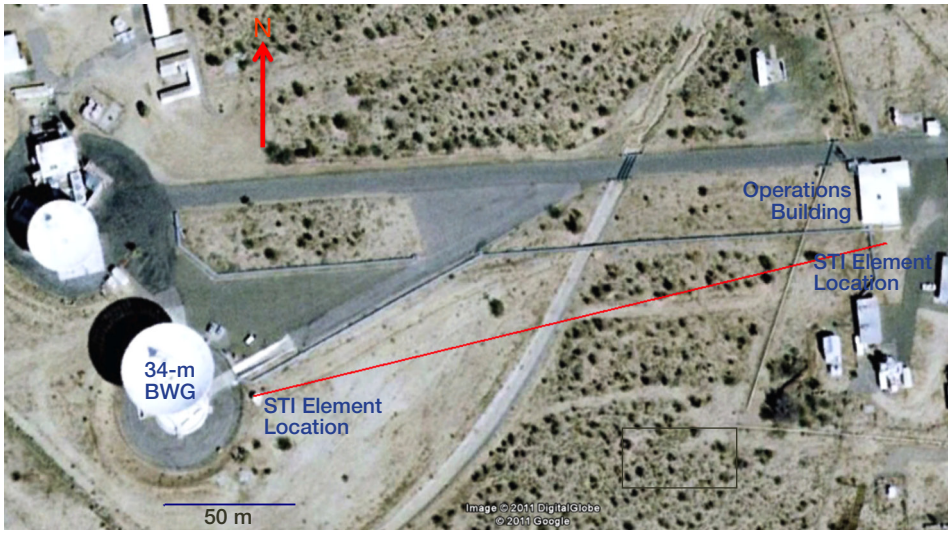

Figure 1. Satellite image of Venus site showing locations of the two STI elements on an approximately east–west baseline with a superimposed red line connecting the two elements. The image was taken prior to deployment of the STI. Image: Google Earth™ mapping service.

A second STI was deployed at Goldstone in September 2010 at the Apollo site (latitude of 35.16 deg N and longitude 243.125 deg E) where the DSN has three operational 34-m-diameter BWG antennas. The Apollo STI is located about 12.5 km away at a heading of 324 deg with respect to the Venus STI. The Apollo subnet is a candidate for X-band uplink array activities and has been used for X-band uplink array demonstrations [1]. Figure 2 shows the locations of the two STI elements (antennas and equipment boxes) residing at Apollo overlaid onto a satellite image of the site. One element is located 50 m south of a 34-m antenna and the other is located on the south side of the foundation pad of a 12-m antenna.

After examining several existing designs, the Harvard-Smithsonian Center for Astrophysics (CfA) design was selected for this STI. This design is of an equal-arm white noise interferometer making use of a satellite's wideband digital TV broadcast signals. Direct-broadcast TV signals have high power and provide higher signal-to-noise ratio than do the narrowband beacon tones used by other STI designs, given practical receiver bandwidths. Use of wideband signals also discriminates against signals arriving from directions different from the desired one, including multipath reflections and other satellites residing in nearby orbital positions.

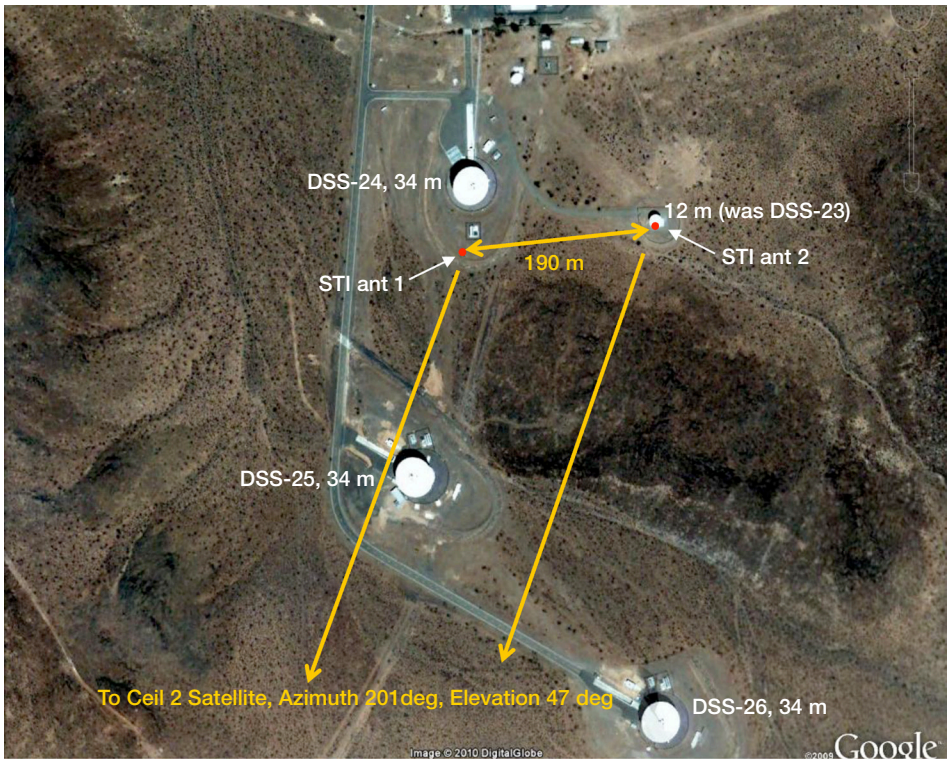

Figure 2. Photo of the Apollo STI site at Goldstone showing the locations of the two elements, their baseline, and the direction to the Ciel 2 geostationary broadcast satellite. North is up. Image: Google Earth™ mapping service.

An STI of this design has been successfully operating at the site of the Sub-Millimeter Array (SMA) at Mauna Kea, Hawaii. Other designs that were considered were found to be older and more difficult to duplicate without significant redesign. The CfA design, with some modifications, was used for the prototype system deployed at the Goldstone Apollo site, and four production systems, which include two systems, one of which was deployed at the Canberra DSN complex and another to be deployed at the Madrid DSN complex, and two systems built under separate contract for deployment to candidate Square Kilometer Array (SKA) sites in Australia and South Africa.

The two 0.84-m-diameter antenna elements and associated electronics receive the RF broadband signals emitted by the Ciel 2 geostationary broadcast satellite (orbital longitude of 129 deg W) at an elevation angle of 47 deg and frequency of 12.5 GHz. The signals are downconverted at each antenna to an IF of 1.2 GHz using an LO signal distributed from a common oscillator over optical fibers. The IF signals are brought to an indoor signal processing rack on separate optical fibers where they are cross-correlated using an analog I-Q mixer, producing in-phase and quadrature-phase components of the cross power. The IF fiber lengths were chosen to equalize the total signal delays input to the mixer, accounting for the difference in free-space delay from the satellite to the antennas.

The I-Q mixer outputs are digitized and averaged over each 0.1-s interval; these are the raw observables of the instrument, which are recorded in real time to a local disk drive, and then periodically downloaded via TCP/IP connections to other computers for analysis.

Some processing is done in real time, but most analysis takes place off-line. Some additional files containing ancillary housekeeping information are also produced by the STI.

Data are also downloaded that are available from other instruments at the site or nearby, such as from water vapor radiometers (WVRs) and meteorology stations. These data can then be compared with the STI data. The Goldstone Apollo STI routinely began data acquisition shortly after completion of its deployment and testing activities starting on September 21, 2010.

III. STI Delay Statistics

The data from the Venus and Apollo STIs are both closely examined and compared on a periodic basis to evaluate the consistency of the two Goldstone data sets. The Venus STI measures in-phase (I) and quadrature-phase (Q) components of the baseband signal with respect to the receiver's local oscillator, separately for each antenna, every 1.0 s. The Apollo STI measures the in-phase (I) and quadrature-phase (Q) cross-correlation of its two IF signals every 0.1 s. In each case, the four-quadrant phase angle $atan\left(\frac{Q}{I}\right)$ is computed; for the Venus STI, the phases of the two antennas are then subtracted. The resulting time series is then phase-unwrapped by adding 2π for each completed cycle.

The contributions of long-period satellite motion and instrumental drift are estimated using a second-order polynomial fit over each 600-s block of data. An example of the corrected output phase for a one-day time period from the Apollo STI is shown in Figure 3 along with the fitted model phase for each 600-s interval. The measured phase and model phase lie on top of each other in this plot, and thus their differences are not discernible on this scale. The diurnal sinusoidal variation in the phase seen in Figure 3 is due to satellite motion,

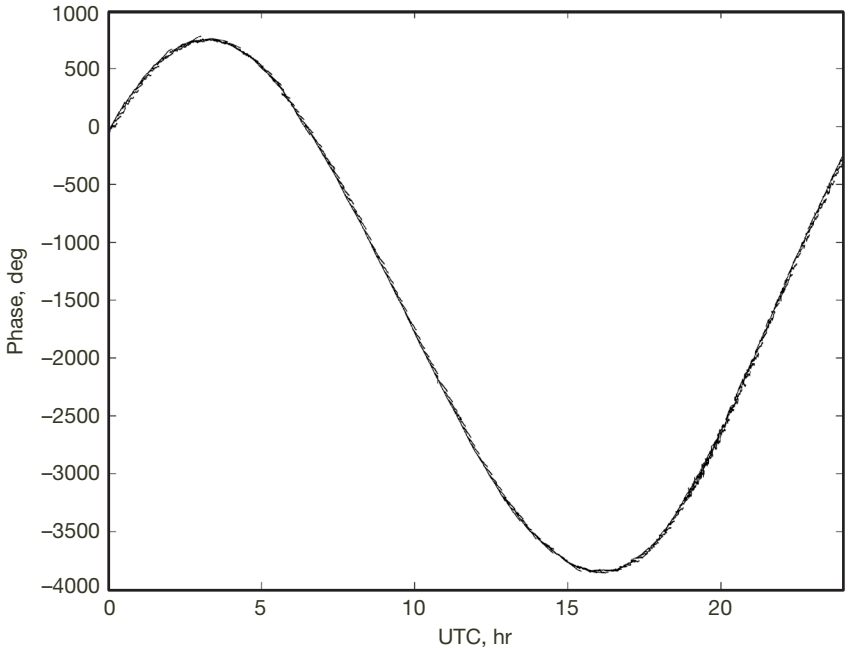

Figure 3. Measured and model phases for September 25, 2010, from Apollo STI.

which is small compared to the beams of the individual antennas, thus allowing each antenna to be fixed. There may also be instrumental drift in the phase due to environmental disturbances or component aging.

The fitted model is then subtracted from the data, and the residual is assumed to be dominated by tropospherically induced fluctuations. These fluctuations are characterized by the standard deviation of the residual phase over each 600-s block of data ($\sigma_{\Delta\phi}$). Thus, there are 144 $\sigma_{\Delta\phi}$ estimates for a one-day period.

The 600-s analysis interval was initially selected for the routine Venus STI data processing based on a rationale discussed in [7]. Since the Apollo STI has a similar element spacing (191 m), it was decided that using 600-s blocks for the Apollo data processing would be reasonable to facilitate comparison using equal duration blocks between STIs. Future analyses may consider other filtering techniques and block sizes.

The line-of-sight measurements of $\sigma_{\Delta\phi}$ from each STI are converted to standard deviation of zenith delay as $\sigma_{\Delta\tau} = \sigma_{\Delta\phi}\sin(\theta)/f_{STI}$, where θ_{STI} is the elevation angle of the observed satellite and f_{STI} is the center frequency of the observed signal. The variation in $\sigma_{\Delta\tau}$ shown in Figure 4 is typical, in that lower values occur during the quieter, cooler nighttime periods and the higher values occur during the daytime when the atmosphere is usually warmer and more turbulent. The $\sigma_{\Delta\tau}$ statistics can be examined on a monthly basis as well as between day and night, between seasons, or from year to year. Its cumulative distribution can also be made available in tabular form in documents such as [9] for look-up for use in spacecraft array link budget calculations for a particular array configuration. Here, the statistics are translated to the link frequency and elevation angle of interest and then scaled to the baseline of each element pair in an array [2–4]. The $\sigma_{\Delta\tau}$ series can also be used to compare STIs within the same site (see Figure 5).

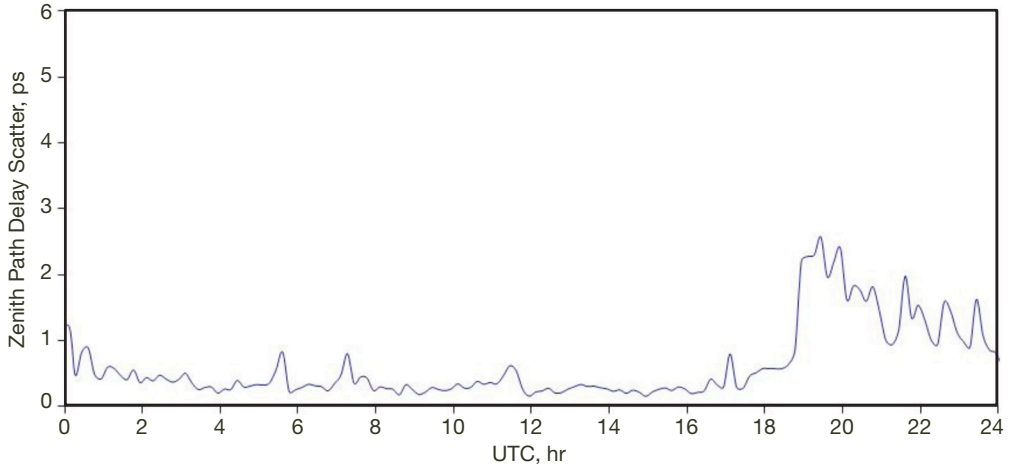

Figure 4. Standard deviation of residual zenith delay in each 600-s interval derived from raw data in Figure 3.

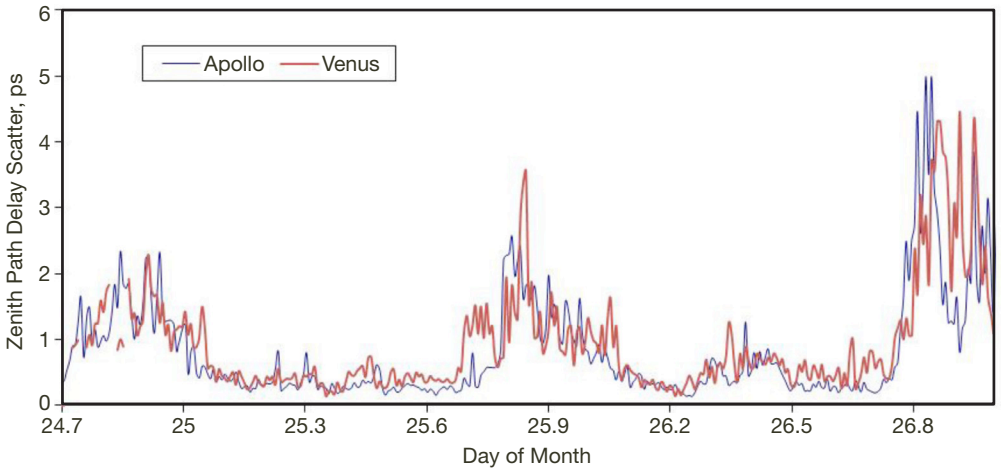

Figure 5. A sample two-day period in September 2010 of $\sigma_{\Delta\tau}$ estimated over 600-s time blocks for both STIs: Apollo (blue) and Venus (pink).

Figure 6 displays an image of the Goldstone complex showing relative locations of the Venus and Apollo STIs. These two instruments are separated by ~12.5 km and each is located in a different terrain. The $\sigma_{\Delta\tau}$ signatures from the two STIs shown in Figure 5 follow each other reasonably well given the distance between them, providing insight and confidence on how a single STI may do a reasonable job of characterizing a site. The statistics for this common data period are presented in Table 1 for both STIs as well as the ratios. It should be noted that the Venus STI data had an additional correction where an estimate of thermal noise of 0.158 ps was removed in a quadratic fashion. Plots such as Figure 5 can provide confidence and validation checks for the data sets as well as being useful for revealing anomalies.

The STI data from two widely spaced locations are thus expected to be in general statistical agreement, but their temporal signatures could also show differences due to passage of weather systems and effects of terrain. When examining the time series of the standard deviations of the path delays over 600-s periods ($\sigma_{\Delta\tau}$) between spatially separated STIs, one expects better agreement during cooler quiet periods such as nighttime and winter, and larger differences between the two data sets during warmer, more turbulent, weather conditions such as summer days. During warmer periods, large differences between data are expected to be due to effects of local terrain coupled with differences in local weather (wind speeds/directions) that may impact the observations in different ways. One also expects to see the delayed effects of large storm cells as they propagate over the complex. Such effects can be correlated with local weather data (e.g., wind speed and direction) and nearby WVR data (e.g., retrieved path delay).

The final product of the first stage of data processing is 144 blocks of filtered data for each full day; from these we can generate statistics, including the standard deviation of each block. The time series of the standard deviation for the winter month of December 2008 is shown in Figure 7. These data are representative of a long "quiet" month marked by less turbulent conditions as it was colder and there was less water vapor present in the atmo-

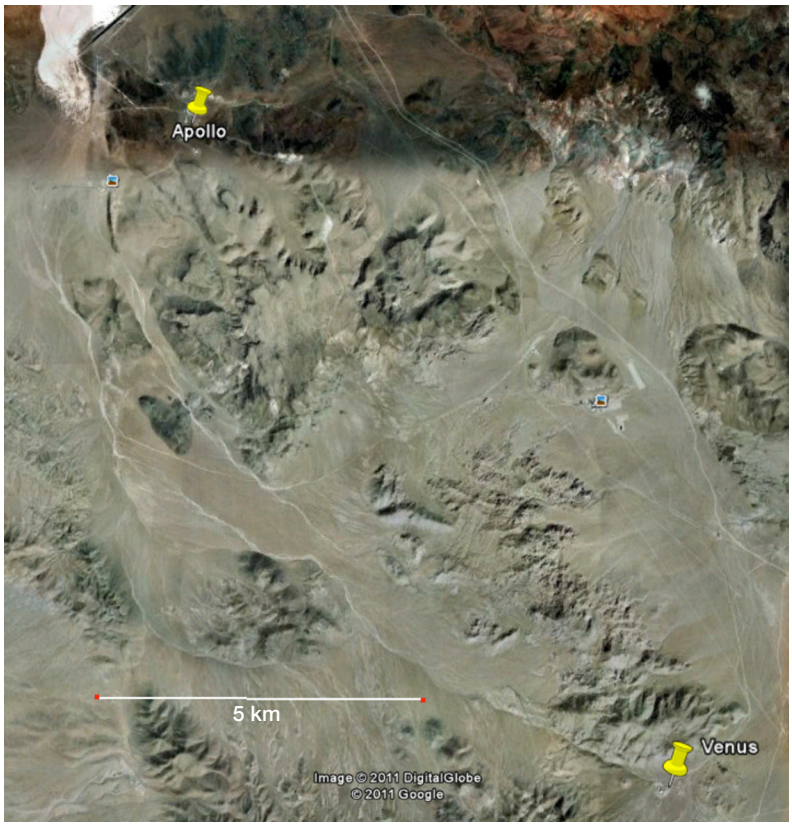

Figure 6. An image of the Goldstone, California, complex showing locations of Venus and Apollo STIs along with terrain. Image: Google Earth™ mapping service.

Table 1. Goldstone STI $\sigma_{\Delta\phi}$ statistics for common data periods shown in Figure 5.

STI	Minimum	Maximum	Average	Units
Apollo	0.14	4.99	0.83	ps
Venus	0.14	4.46	0.93	ps
Venus/Apollo	1.00	0.89	1.13	

sphere. An unusually extended quiet period of data on December 11, 2008 (inside the red rectangle in Figure 7), was the cold, dry day case chosen for detailed analysis of the phasing loss that a two-element array would experience (see Section V).

To assess the upper range of amplitude fluctuations expected from such data, zenith path delay fluctuations measured for one of the warmest months, August 2008, was inspected (see Figure 8). A representative warm, humid day from which to extract two-element amplitude loss from the differenced path delay time series was chosen to be August 29, 2008, shown inside the red rectangle in Figure 8 (see Section V). This data set includes reasonably quiet nighttime summer conditions and larger daytime fluctuations when temperatures are higher and there is more water vapor content and variability present. Thus, August 29, 2008, is representative of warm summer month conditions with diurnal night–day activity characterized by higher levels of delay fluctuations.

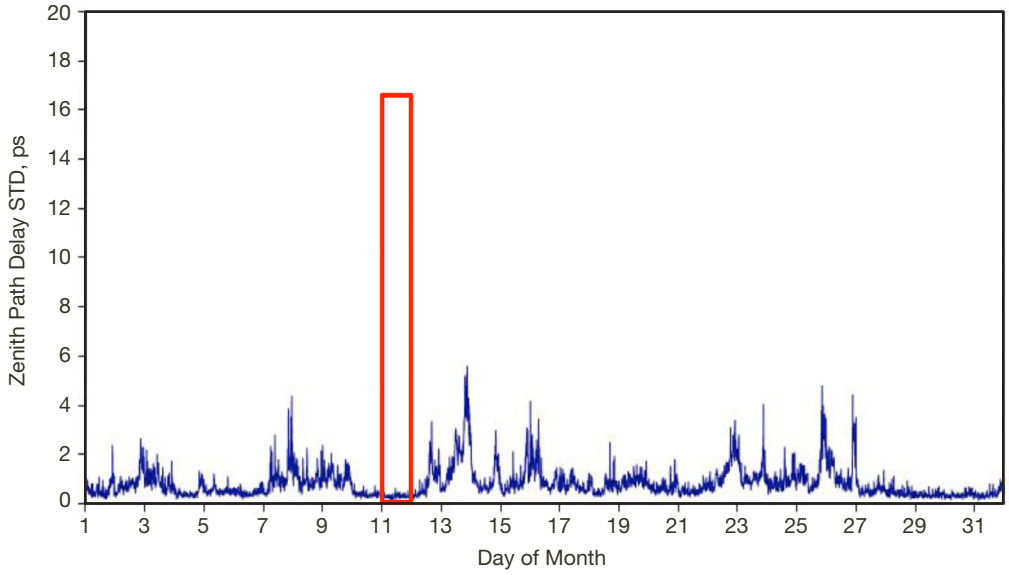

Figure 7. Goldstone Venus STI phase converted to zenith path delay fluctuations in the form of standard deviations from December 2008 served as a cold, dry month case.

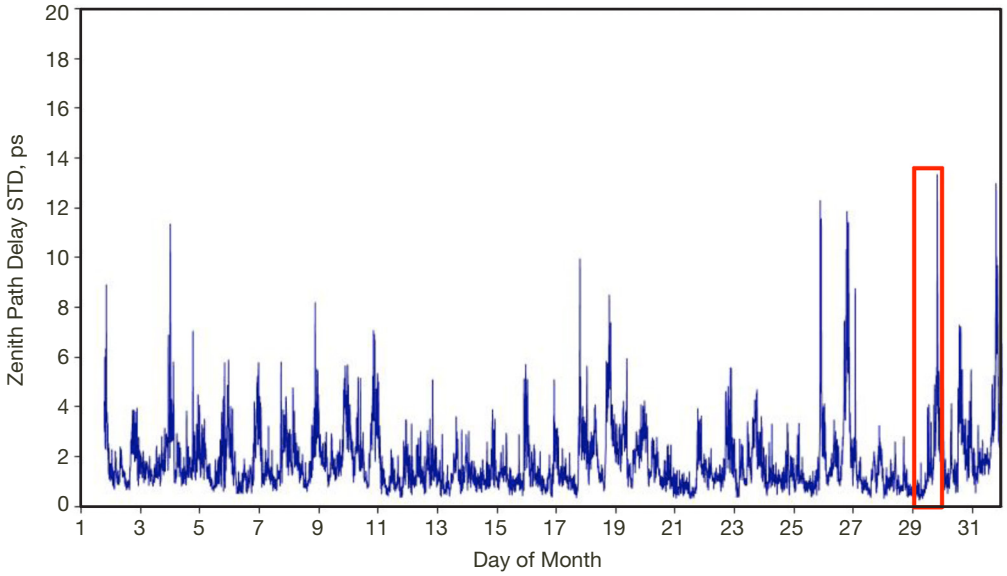

Figure 8. Goldstone Venus STI August 2008 zenith path delay standard deviation data in 600-s blocks that were inspected to find data periods that were representative of summer conditions useful in assessing tropospherically induced fluctuations.

IV. Data Processing and Analysis Approach for Amplitude Loss Characterization

This section describes the estimation of amplitude loss derived from STI phase delay, which will be used for the two representative cases chosen for close analysis (Section V) and for overall amplitude loss statistics (Section VI).

The time series of the STI residual phase observations after subtraction of the fitted model phase at the STI frequency f_{STI} and STI elevation angle θ_{STI} are referenced to the link frequency and elevation angle of interest as follows:

$$\Delta\phi_{link} = \Delta\phi_{sti}\left[f_{link}/f_{STI}\right]\left[\sin(\theta_{STI})/\sin(\theta_{link})\right] \quad (1)$$

where $\Delta\phi_{link}$ is the STI phase difference at the desired link frequency f_{link} and elevation angle θ_{link}.

The Venus STI link frequency f_{STI} is 20.2 GHz, the beacon frequency emitted by the ANIK F2 satellite. The Apollo STI link frequency f_{STI} is 12.5 GHz, the approximate center frequency of the wideband digital TV signals emitted by the Ciel 2 broadcast satellite. The link frequency, f_{link}, in which we are interested for examining amplitude loss, is the nominal DSN uplink X-band frequency of 7.15 GHz.

The Venus STI elevation angle to ANIK F2 is 48.5 deg. The Apollo STI elevation angle to Ciel 2 is 47.1 deg. The link elevation angle in which we are interested for examining amplitude loss is 20 deg, which is a nominal design point defining the worst-case airmass over a tracking pass where an array tracks a spacecraft from 20 deg during rise through meridian transit to 20 deg during set. Such a tracking pass will last several hours depending upon the latitude of the array and declination of the spacecraft.

The residual phase measurements can be scaled to a baseline other than that of the STI. There is both theoretical and experimental evidence that the scaling is of the form

$$\Delta\phi_{link}(r_{ij}) = \Delta\phi_{STI}(r_{sti})\left(\frac{r_{ij}}{r_{sti}}\right)^{\beta/2} \quad (2)$$

where r_{ij} is the new baseline length between elements i and j. The Kolmogorov theory of turbulence predicts this form with $\beta = 5/3$ for $r_{ij} << h$, and $r_{sti} << h$, where h is the thickness of the turbulent air layer, and $\beta = 2/3$ for $r_{ij} >> h$ and $r_{sti} >> h$ [10]. We assume that the scaling exponent used in Equation (2) would be $\beta = 5/3$ since baseline distances are much smaller than 1000 m, a reasonable value for h.

For the purpose of this analysis, we perform an additional adjustment to the Venus STI data from Equation (1) to reference the phase difference to that of the Apollo baseline length of 191 m:

$$\Delta\phi_{link}(r_{Apollo}) = \phi_{link}(r_{Venus})\left(\frac{r_{Apollo}}{r_{Venus}}\right)^{\beta/2} \quad (3)$$

where r_{Venus} = 256 m and r_{Apollo} = 191 m. We assume $\beta = 5/3$.

We calculate amplitude (power) loss (P/Pmax) in dB for the case of a two-element array at different frequencies using the following equation for each point in the time series:

$$\text{Loss}(\text{dB}) = 10\log_{10}(\text{P/Pmax}) = 10\log_{10}\left(\tfrac{1}{2}[1 + \cos\Delta\phi_{\text{link}}]\right) \quad (4)$$

V. Detailed Analysis of Two Selected Days

In order to facilitate the analysis of the effect of tropospheric-induced STI phase variations on two-element phasing loss, we selected two days of data from the Goldstone Venus STI data archive for detailed analysis as previously described; one cold-weather day on December 11, 2008, where amplitude fluctuation effects due to troposphere were expected to be near minimum and one hot, humid day on August 29, 2008, where such effects were expected to be near maximum. These two cases are expected to be representative of the range of conditions over which amplitude loss can be characterized.

For the case of the cold, quiet day of December 11, 2008, the amplitude loss estimates (see Figure 9) were calculated from the STI phase difference time series via use of Equations (1), (3), and (4). We see that with the exception of three anomalous points in Figure 9 (where one is located at the right edge of the plot), all of the amplitude loss estimates lie well below 0.05 dB at 7.15 GHz, 20-deg elevation angle, and scaled to 191 m element separation. Thus, at X-band, the atmospheric degradation on the two-element amplitude, when arraying two antennas during winter coldest conditions, is shown to be very small. The corresponding structure function is shown in Figure 10. Here we see that the slope $\beta \sim 2/3$ at time intervals less than 20 s is consistent with thin-shell Kolmogorov theory, which is representative of conditions when the upper edge of the turbulent layer lies at an altitude that is smaller than the element separation of the STI.

For the case of the warm, humid weather day example, August 29, 2008, we see from Figure 11 that all amplitude fades lie below ~0.1 dB in attenuation for the first half of the day, which is mostly nighttime. Higher phasing loss is evident during the daytime period of the last 12 hr with occasional losses of up to 3 dB, except during 19:00 to 20:00 UTC where there are huge phasing losses of up to several tens of dBs. The slope of the structure function for the data of August 29, 2008, lies between that of the thin model ($\beta = 2/3$) and thick model ($\beta = 5/3$), as expected for a mixture of calmer nighttime conditions and more active daytime conditions (see Figure 10).

A close-up examination of ~1 dB fade features near 11:45 UTC in Figure 11 is shown in Figure 12 on an expanded scale (540 s). There appear to be two features of about ~90 s duration each of about 1 dB with smaller features on either side. These features appear consistent with that of a tropospheric origin and can be correlated with other ancillary data types. For instance, these features coincide with abrupt changes in surface meteorological data obtained from two independent weather stations at the site. Wind data from two independent sets of sensors at DSS-13 were examined at the time of these fades. One weather station was the DSN complex instrument located on a nearby tower, which provided both wind speed and wind direction data during the period of the fades as shown in Figures 13(a) and 13(b), respectively. The other weather station, located on the roof of the Venus control building

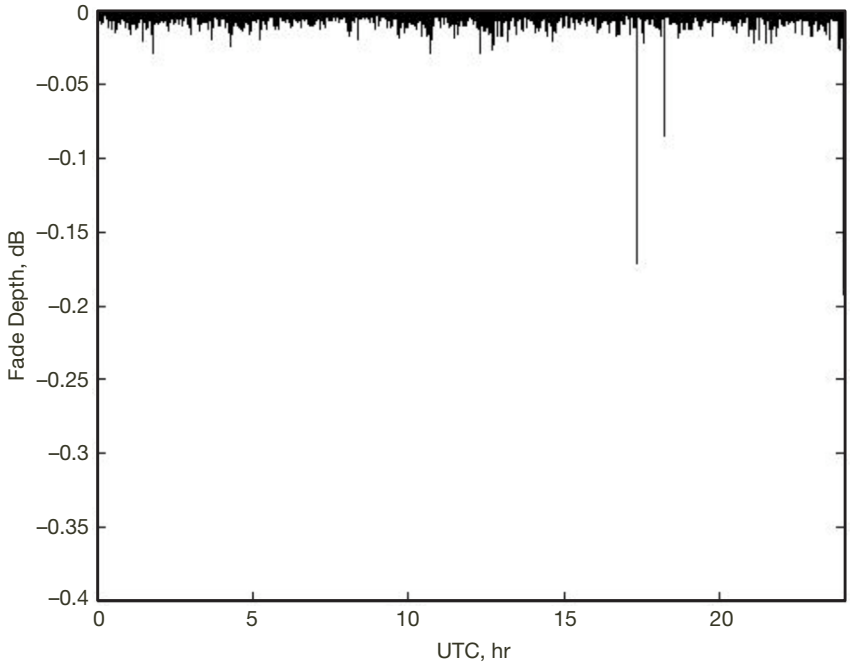

Figure 9. Two-antenna phasing loss estimated from STI phase difference observables for December 11, 2008, referenced to a 7.15-GHz uplink frequency and a 20-deg elevation angle.

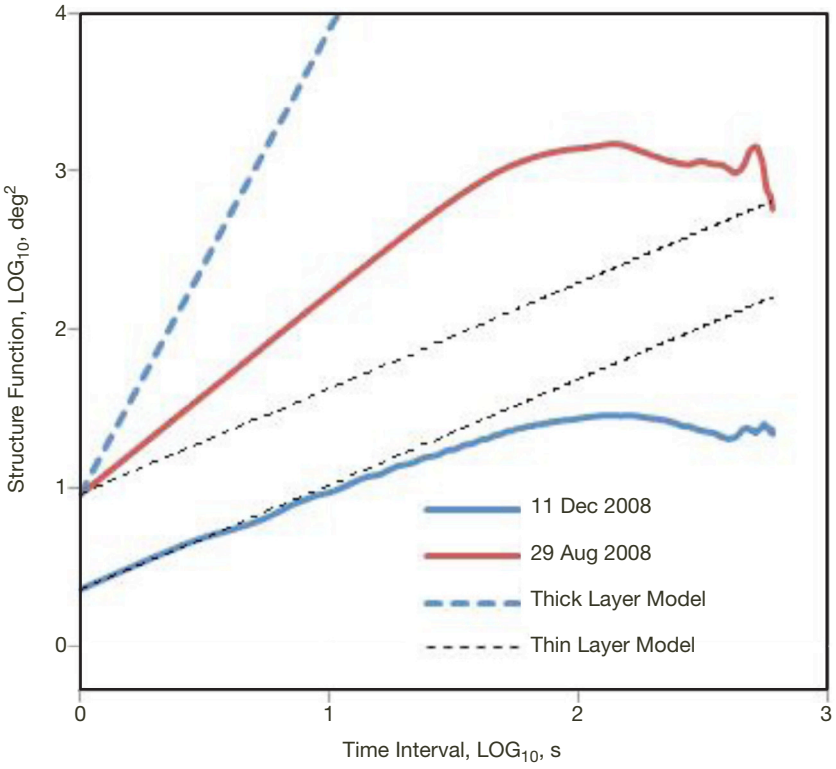

Figure 10. Structure functions for August 29, 2008, and December 11, 2008, data with model curves for β = 2/3 (thin layer) and β = 5/3 (thick layer) slopes.

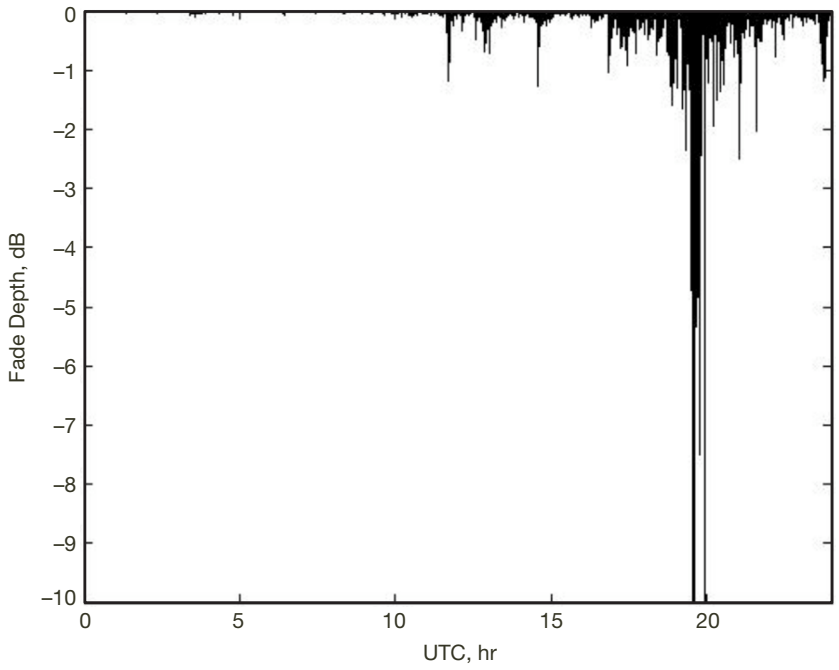

Figure 11. Amplitude phasing loss for two-element array for warm, humid day August 29, 2008, referenced at 7.15 GHz and at a 20-deg elevation angle.

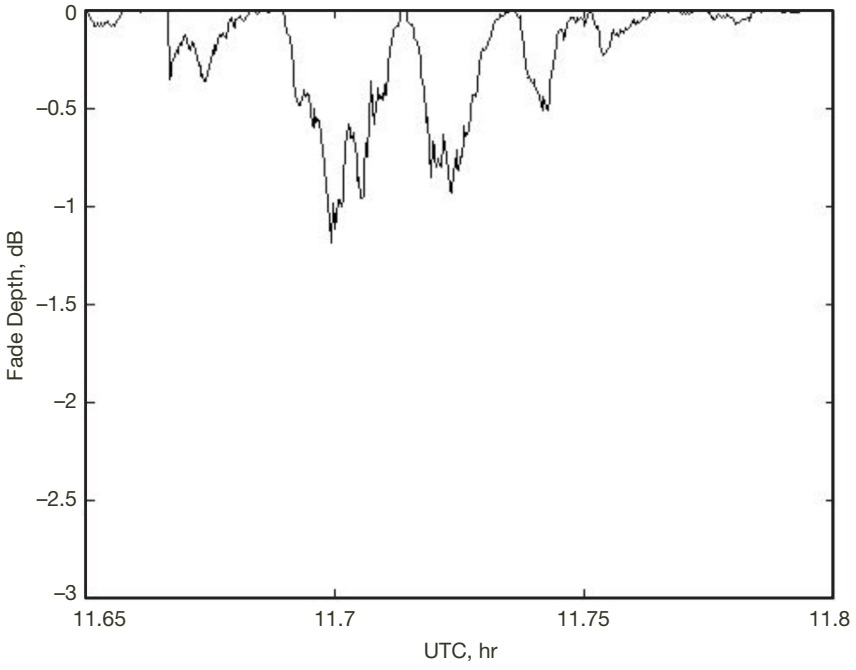

Figure 12. Fade features during August 29, 2008, 11:45 UTC on an expanded scale.

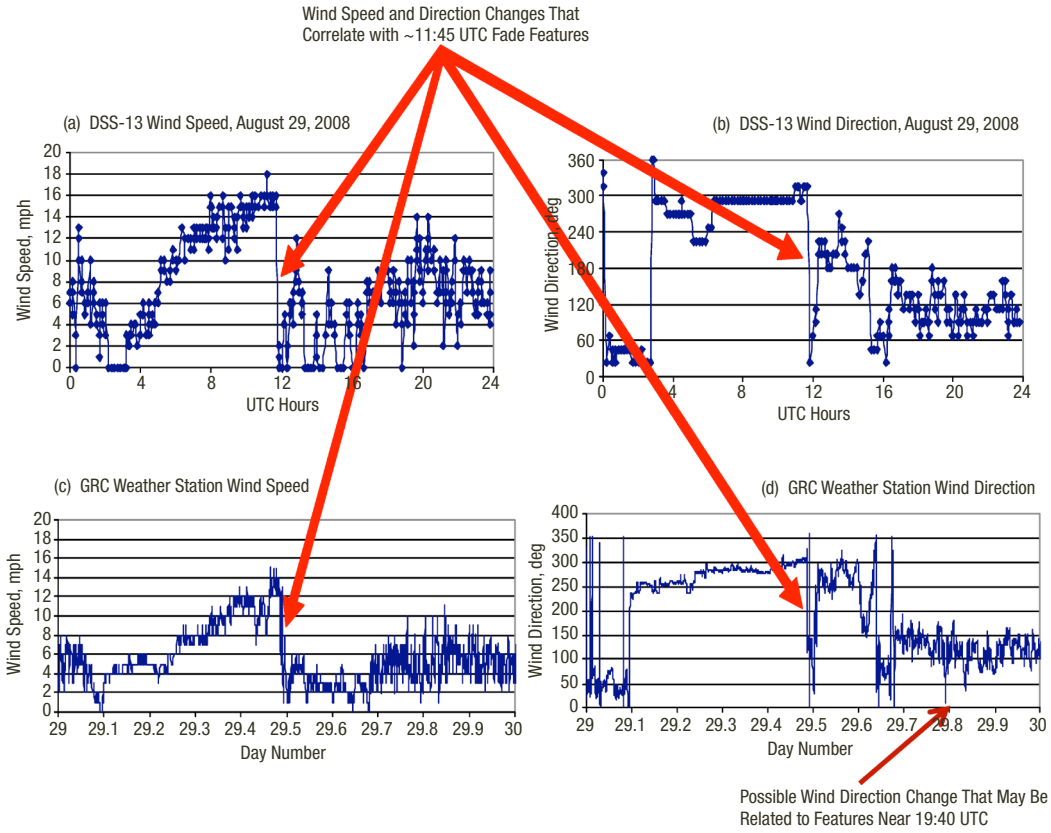

Figure 13. Wind speed and wind direction data from two independent sets of weather sensors at Venus Goldstone site for August 29, 2008: (a) DSS-13 wind speed, (b) DSS-13 wind direction, (c) GRC wind speed, and (d) GRC wind direction. The time axes for both weather stations cover the same period but the time units are different. The time of abrupt changes in wind speed and direction of Figure 12 fade features are indicated by solid red arrows.

and belonging to NASA GRC, provided both wind speed and wind direction data for the time same period as shown in Figures 13(c) and 13(d), respectively. Both sets of weather station wind data show similar behavior with differences attributed to the fact that the stations are located at different places within the complex, and each instrument has different calibration, quantization, and resolution characteristics. Upon inspection of Figure 13, we note that the wind speed was at a sustainable 16 to 18 mph consistently out of the west (300 deg azimuth) and then underwent a dramatic reduction at the time of the fades to much smaller values and changing wind direction readings near 60 deg, which then climbed back up approaching the original 300 deg azimuth but with more pronounced difference between the two sensors at lower wind velocities.

It thus appears that these features shown in Figure 12 may be related to an abrupt change in weather conditions at the site. The wind data from both GRC and DSN sensors are in reasonable temporal agreement, and both indicate a sudden significant shift in conditions just before the onset of the large fade features (indicated by solid red arrows on each plot). This suggests that the 90-s fade features may related to these weather condition changes.

Although many of the smaller ~dB fade features for the August 29, 2008, data can easily be attributed to the troposphere, the much larger several tens of dB fades, such as those near 19:40 UTC in Figure 11, merit further examination to determine whether they can be tropospheric in nature. An expanded scale view of some of these features is shown in Figure 14 over 540 s. We took the raw phase time series and fitted model time series for August 29, 2008, shown in Figure 15 and examined the period about the largest fade features on an expanded scale as shown in Figure 16. The period in question between 19.55 and 19.67 UTC hr (~19:40 UTC) shows detail of the difference between the observed phase and the fitted polynomial model.

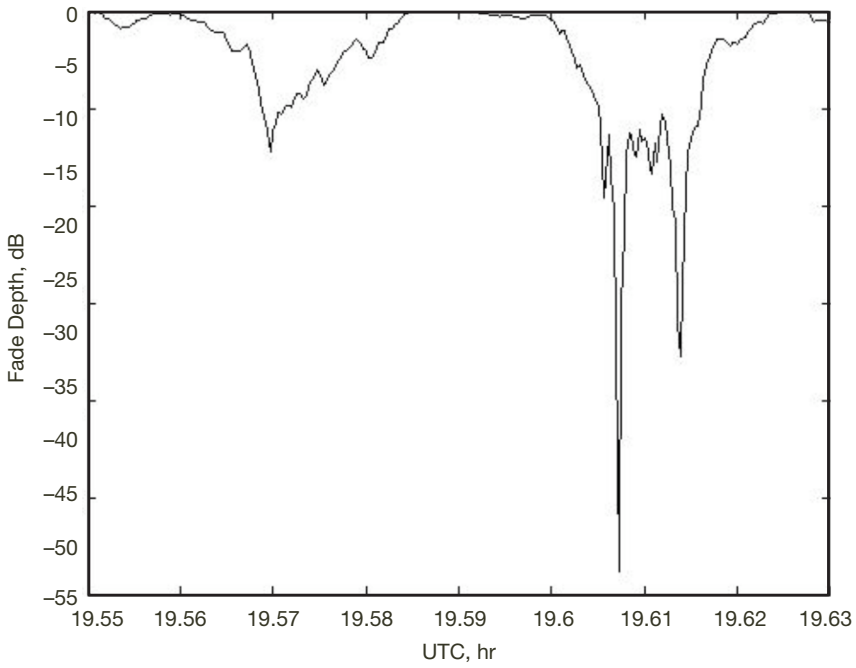

Figure 14. Fade features near 19:40 UTC during August 29, 2008.

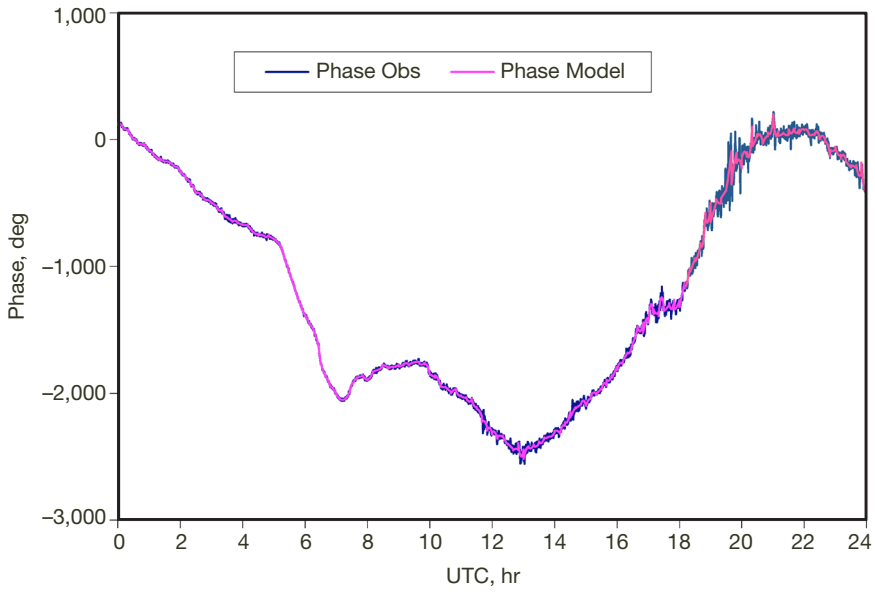

Figure 15. Venus STI August 29, 2008, raw phase (blue) and fitted model phase (pink).

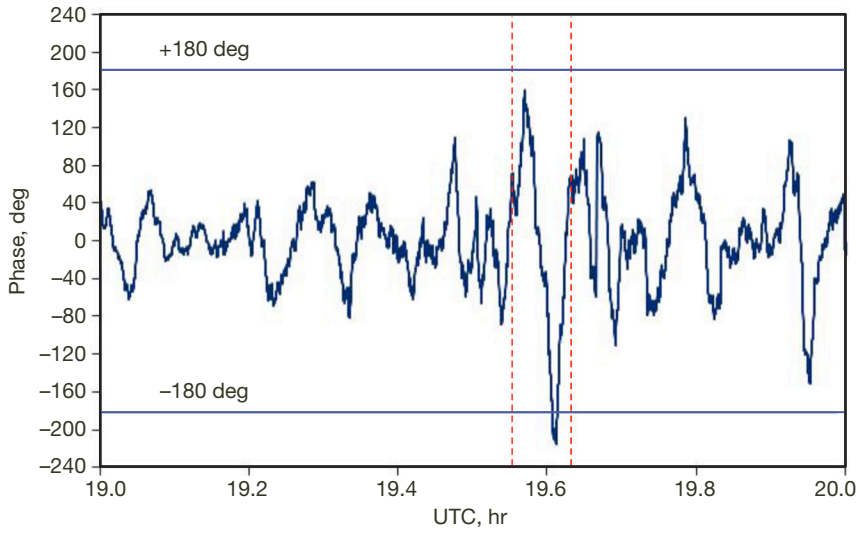

Figure 16. Venus differenced phase (raw–model) from data of Figure 15 covering the period from 19:00 to 20:00 UTC on August 29, 2008. The time interval of Figure 14 is shown between the two dashed vertical red lines. The two instances of large fade values exceeding 30 dB in Figure 14 occur where the differenced phase crosses –180 deg in this figure.

Assuming a 1000-m turbulent air layer thickness, a total phase reversal at the X-band frequency of 7.15 GHz corresponds to a change in integrated refractive index of $\Delta n \sim 0.00002$. Given that the index of refraction for air is typically ~1.0003, the contribution due to water vapor on a warm day is ~0.00017, assuming a partial vapor pressure of 40 mb estimated from the station's surface meteorological data at an air temperature of 300 K. Thus a change of the integrated refractive index due to water vapor ~0.00002 is feasible over the spatial distance of 200 m on these several-minute timescales. There is a small feature in the surface wind data from one sensor (Figure 13d) that suggests a rapid change of wind direction about the same time of the large fades near 19:40 UTC, perhaps reminiscent of activity farther aloft along the satellite line of sight. There is also a large feature in differenced path delay standard deviation (over 600 s data) from the DWVR instrument that coincides with these fades, suggesting significant water vapor variation over the interferometer spacing. There is no evidence of appreciable liquid content along the signal path based on retrievals from the two nearby WVRs or rain gauge data from the surface meteorological data sensors. A closer examination on the nature of these large fade features constituting much less than 1 percent of the data is a focus of future study.

There is no obvious event in the surface meteorological data that can be correlated with these huge fades near 20:00 UTC. Whether or not these events near 19:40 UTC are tropospheric in origin, the overall amount of data with fades exceeding 3 dB do not constitute a significant fraction of the total data, and their inclusion or removal will not perceptibly affect the amplitude loss statistics (see next section). These fade features appear to be associated with slow phase variations that occur over reasonably long time scales (~90 s) (see Figure 14). By far the deepest fade features exceeding 30 dB in Figure 14 are associated with the X-band equivalent phase $\Delta\phi_{link}$ in Equation (3) crossing ~180 deg. The occurrence of such events is rare but possible at X-band. It should be noted that such rare events on a two-element array are even more unlikely to occur with arrays of three or more elements.

VI. Amplitude Loss Statistics

For several months of Venus and Apollo STI data, we calculate the two-element phasing loss referred to a frequency of 7.15 GHz and an elevation angle of 20 deg using the approach discussed in Section IV. We have also made an adjustment for the baseline distance differences for the Venus data to refer it to the Apollo two-element separation distance of 191 m. We first calculated and plotted the cumulative distribution of the two-element phasing loss in dB from the Venus data for selected months as shown in Figure 17. One general result is that for the summer months (Venus STI data), the dB loss at 90th percentile ranges from roughly 0.08 to 0.12 dB — see Figure 17(a). The cooler-month statistics (Venus STI data) show phasing loss at 90th percentile ranging from ~0.01 dB to ~0.05 dB — see Figure 17(b). These results do not change perceptibly when the data containing the large tens of dB fades (such as August 29, 2008) are included or removed from the data for which statistics are generated.

Figure 18 displays cumulative distributions of two-element amplitude loss for the Apollo STI since its September 2010 deployment (solid curves) along with that from available Venus data (dashed curves). Note that the curves for the coldest winter/autumn months lie to the left and the curves for the warmer spring/autumn months lie to the right. Table 2 displays some important statistics for each month. Fades that lie above 1.2 dB loss occur much less than 1 percent of the time, as indicated by Table 2. It is not clear whether the very small percentage of data marked by huge several tens of dB fades (October, November, and December 2010, and March to June 2011 in Table 2) may be tropospheric in origin, and these data periods are being investigated as a focus for further study. The present results do not perceptibly change when such data are deleted from the statistical characterization. The total number of samples for each month (listed in the second column of Table 2) is indicative of several days for which data were lost due to various hardware and procedural issues that have since been addressed and will be described in detail in a future article.

VII. Conclusions

Site test interferometers (STIs) have been deployed at the Venus and Apollo antenna sites in Goldstone, California, to assess the suitability of Goldstone as an uplink array site, and to statistically characterize atmospheric-induced phase fluctuations for application to Goldstone array link scenarios. The fluctuation in delay statistics derived from the STI data sets was mapped into two-element amplitude fades at a frequency of 7.15 GHz, at an elevation angle of 20 deg, and a baseline separation of 191 m to assess statistical behavior for possible future array activities. For warm months, the loss at 90th percentile ranged from roughly 0.08 to 0.12 dB. For cool months, the loss at 90th percentile ranged from just above 0.01 dB to 0.05 dB. Some issues related to several periods of significant tens of dB loss are being investigated. The removal of these data is not expected to significantly change these results. Results such as these can be used to statistically quantify phasing loss for future array configurations using the Goldstone tracking site.

(a)

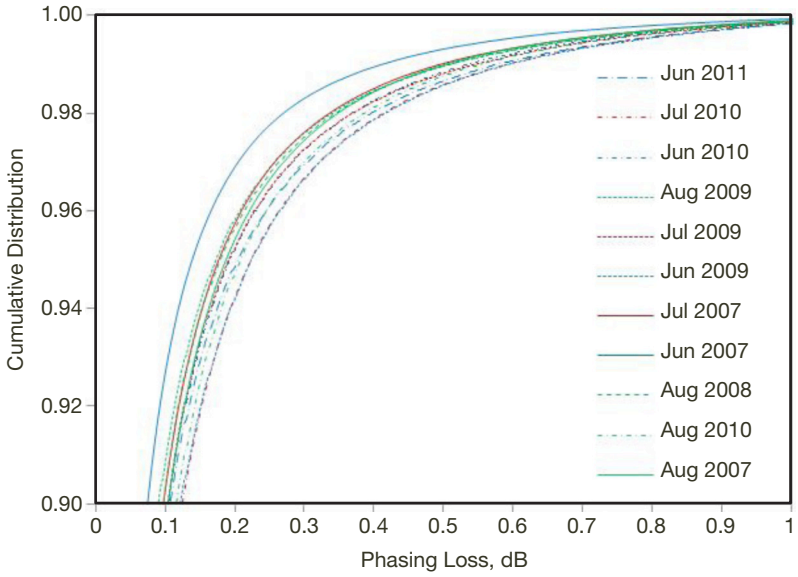

(b)

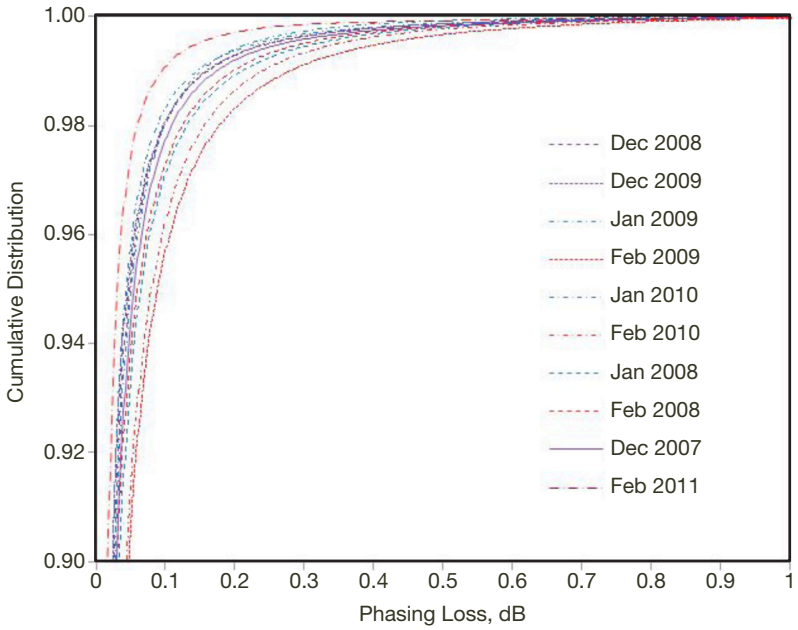

Figure 17. Two-element phasing loss cumulative distributions calculated for 7.15 GHz frequency, 20-deg elevation angle, and 191 m separation for selected months: (a) summer months; (b) winter months.

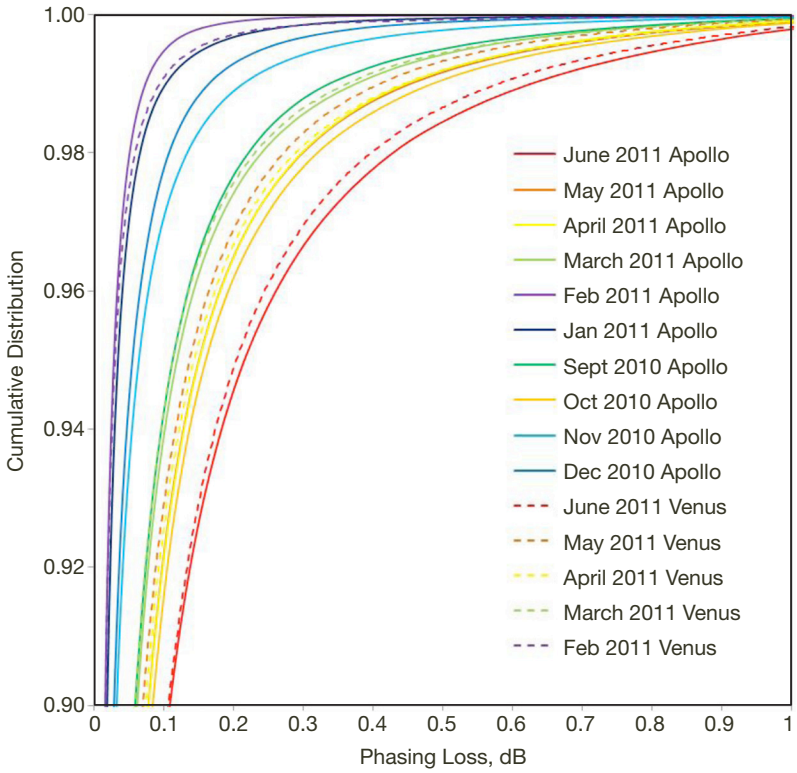

Figure 18. Monthly cumulative distribution curves for Apollo STI baseline data calculated for 7.15 GHz frequency, 20-deg elevation angle, and 191 m antenna separation.

Table 2. Apollo STI phasing loss statistics.*

Month	Total Number of Samples	Percent <1.2 db	Maximum dB Sample
September 2010	8621771	99.90	4.0
October 2010	19767868	99.67	68.0
November 2010	25860975	99.94	39.9
December 2010	13576405	99.88	96.7
January 2011	24319713	99.99	6.4
February 2011	9580448	100.00	12.6
March 2011	19864853	99.88	44.3
April 2011	24499158	99.80	70.1
May 2011	26111350	99.62	99.2
June 2011	21915737	99.22	87.0

* Calculated for 7.15 GHz frequency, 20-deg elevation angle, and 191 m antenna separation.

Acknowledgments

We would like to thank Faramaz Davarian and Barry Geldzahler for support of this work; Vahraz Jamnejad for providing valuable comments on the manuscript; and Roberto Acosta and James Nessel of NASA GRC for use of the GRC STI and weather station data taken at the Venus Goldstone site.

References

[1] V. Vilnrotter, D. Lee, T. Cornish, P. Tsao, L. Paal, and V. Jamnejad, "Uplink Array Concept Demonstration with the EPOXI Spacecraft," *Proceedings of the 2009 IEEE Aerospace Conference*, paper 4.0101, Big Sky, Montana, March 7–14, 2009.

[2] D. D. Morabito and L. D'Addario, "Site Test Interferometer Atmospheric Decorrelation Statistics Use in Uplink Array Link Budgets," *Proceedings of 13th Ka and Broadband Communications Conference*, Turin, Italy, September 24–26, 2007.

[3] D. D. Morabito, L. D'Addario, S. Shambayati, R. J. Acosta, and J. A. Nessel, "Goldstone Site Test Interferometer Atmospheric Decorrelation Statistics Use in Spacecraft Link Budgets: First Year of STI Data," *Proceedings of the 14th Ka and Broadband Communications Conference*, Matera, Italy, September 24–26, 2008.

[4] L. R. D'Addario, "Combining Loss of a Transmitting Array due to Phase Errors," *The Interplanetary Network Progress Report*, vol. 42-175, Jet Propulsion Laboratory, Pasadena, California, pp. 1–7, November 15, 2008.
http://ipnpr.jpl.nasa.gov/progress_report/42-175/175G.pdf

[5] R. J. Acosta, B. Frantz, J. A. Nessel, and D. D. Morabito, "Goldstone Site Test Interferometer," *Proceedings of the 13th Ka and Broadband Communications Conference*, Turin, Italy, September 24–26, 2007.

[6] J. A. Nessel, R. J. Acosta, and D. D. Morabito, "Goldstone Site Test Interferometer Phase Stability Analysis," *Proceedings of the 13th Ka and Broadband Communications Conference*, Turin, Italy, September 24–26, 2007.

[7] R. J. Acosta, J. A. Nessel, and D. D. Morabito, "Data Processing for Atmospheric Phase Interferometers," *Proceedings of the 14th Ka and Broadband Communications Conference*, Matera, Italy, September 24–26, 2008.

[8] J. A. Nessel, R. J. Acosta, and D. D. Morabito, "Phase Fluctuations at Goldstone Derived From One-year Site testing Interferometer Data," *Proceedings of the 14th Ka and Broadband Communications Conference*, Matera, Italy, September 24–26, 2008.

[9] *DSN Telecommunications Link Design Handbook*, DSN No. 810-005, Jet Propulsion Laboratory, Pasadena, California, April 29, 2011.
http://eis.jpl.nasa.gov/deepspace/dsndocs/810-005/

[10] C. Coulman, "Fundamental and Applied Aspects of Astronomical Seeing," *Annual Review of Astronomy and Astrophysics*, vol. 23, pp. 19–57, 1985.